forum acusticum 2026
8-12 September · Graz, Austria

SONIC BLACK HOLES FOR ENHANCING DETECTION OF WEAK SIGNALS

Semere B. Gebrekidan[1], Florian Toth[1]
[1] *Institute of Mechanics and Mechatronics, TU Wien, Austria*

This paper is a revised version of the authors' submitted manuscript that was peer-reviewed by at least two anonymous reviewers.

Abstract

Acoustic wave propagation inside sonic black holes (SBHs) is characterized by a decrease in the speed of sound and a gradual increase in pressure magnitude. Besides their application as broadband sound absorbers, this paper explores their use as broadband pressure enhancement devices to improve the detection of weak signals by exploiting the gradual increase in pressure magnitude. We numerically and experimentally demonstrate an enhancement of up to 20 dB in signal detection by placing a microphone inside the SBH, and compare its performance with that of a microphone in a free field. This approach paves the way for passive acoustic wave amplification of weak signals, enabling low-power devices with enhanced detection capability.

Keywords: *acoustic, weak-signal, amplification, sonic-black holes*

1. Introduction

The detection of acoustic wave signals is limited by the sensitivity of the acoustic sensor and the strength of the signals. In the case of weak signals, distinguishing from background noise becomes challenging and requires advanced signal processing to recover the original signal. In addition, active control methods can amplify weak signals, as in many applications, such as hearing aids. However, to further enhance the detection of weak signals, it is essential to amplify the acoustic wave before it reaches the receiver. In recent years, acoustic metamaterials have been employed to improve the detection limits of weak signals by exploiting acoustic resonance [1]; however, this approach is typically limited to narrow frequency bands. By gradually varying the effective refractive index using gradient structures, which leads to wave compression and pressure amplification, broadband devices for enhancing weak signals have been demonstrated [2], [3], [4]. However, the thickness of such broadband structures generally increases with bandwidth and performance. Therefore, an important question remains: how can the detection limit of weak signals be enhanced over a broad bandwidth with limited thickness, without relying on active electro-acoustic devices?

Acoustic black holes are structures with a gradual change in thickness that lead to a gradual increase in wave amplitude and a reduction in the speed of sound. By placing dissipative material at the end, acoustic black holes have been commonly used for vibration reduction [5], [6], [7]. In addition, the increase in amplitude has been used to improve the detection of weak signals of elastic waves over broadband frequencies [8], [9]. In acoustics, such effects are achieved by the gradual reduction of the opening area, resulting in gradual impedance matching, which has been widely used for sound absorption applications by placing dissipative material within the device. Although the term "acoustic black holes" is commonly used, the term "sonic black holes" (SBH) is adopted here to refer to acoustic counterparts and avoid confusion. These structures are commonly used as broadband sound absorbers by incorporating dissipative materials at the termination. Recent works have shown the ideal SBH shapes that lead to better absorption performance and their relation to acoustic wave-focusing characteristics [10]. Recently, SBH-like devices have been demonstrated for acoustic wave focusing through topology optimization [11], [12]. The acoustic pressure distribution inside the optimized SBH shows improvement over conventional ribbed-SBH designs, providing a new perspective on the design of optimal SBH structures for acoustic wave focusing. Following this study, acoustic wave focusing in optimized SBHs has been verified using a laser vibrometer, and the effect of geometric asymmetry on wave focusing has been discussed [13]. To further characterize the optimized SBH devices, the effective speed of sound has been analyzed in the time domain by correlating the peak of the traveling wave

Corresponding author: *semere.gebrekidan@tuwien.ac.at.*

with a reference [14], and the local phase velocity has been evaluated using a three-point method [15], which provides accurate estimation even in the presence of significant reflection.
Based on our previous work [15], where we demonstrated that optimizing the pressure inside the design domain provides improved wave-focusing performance compared to optimizing the transmission bandwidth [12], this paper presents a detailed investigation into the optimization of SBH designs with improved and broadband wave-focusing characteristics, along with numerical and experimental validation of their application to enhance the detection of weak signals in a free field.

2. Method

For plane wave propagation in a 2D axisymmetric waveguide, acoustic topology optimization is formulated in terms of the Helmholtz equation,

$$\nabla \cdot \left(\rho^{-1} r \nabla \hat{p}\right) + \omega^2 \kappa^{-1} r \hat{p} = 0, \tag{1}$$

where the density (ρ) and bulk modulus (κ) are expressed using nondimensional variables $\hat{\rho}$ and $\hat{\kappa}$ [16]:

$$\hat{\rho} = \frac{\rho}{\rho_a} = \begin{cases} 1, & \text{air}, \\ \frac{\rho_s}{\rho_a}, & \text{solid}, \end{cases} \qquad \hat{\kappa} = \frac{\kappa}{\kappa_a} = \begin{cases} 1, & \text{air}, \\ \frac{\kappa_s}{\kappa_a}, & \text{solid}. \end{cases}$$

Substituting these relations into Eq. (1), the dimensionless Helmholtz equation becomes

$$\nabla \cdot \left(\hat{\rho}^{-1} r \nabla \hat{p}\right) + \hat{\omega}^2 \hat{\kappa}^{-1} r \hat{p} = 0, \tag{2}$$

where $\hat{\omega} = \omega/c$, and $c = \sqrt{\kappa_a/\rho_a}$ is the speed of sound in air. The terms ω and c represent the angular frequency and the speed of sound, respectively. Neumann and Dirichlet boundary conditions are imposed on the sound-hard boundary and inlet/outlet boundaries, respectively.
The density distribution within the design space is controlled using $\hat{\rho}(\zeta)$, where ζ is a continuous design variable. A binary final design is achieved when $\zeta = 0$ or $\zeta = 1$, corresponding to solid or air, respectively.
The Solid Isotropic Material with Penalization (SIMP) method, employing inverse material properties, is used to represent the continuous variation between aluminum and air [16]:

$$\hat{\rho}(\zeta)^{-1} = 1 + \zeta \left[\left(\frac{\rho_s}{\rho_a} \right)^{-1} - 1 \right], \tag{3}$$

$$\hat{\kappa}(\zeta)^{-1} = 1 + \zeta \left[\left(\frac{\kappa_s}{\kappa_a} \right)^{-1} - 1 \right]. \tag{4}$$

The optimization problem is formulated to maximize the sum of the absolute total pressures at discrete points within the SBH, subject to lower and upper bounds that enforce an increase in pressure toward the end of the design domain. The design space is divided into 14 discrete points with equal spacing of 0.02 m along an axisymmetric line, as shown in Figure 1.

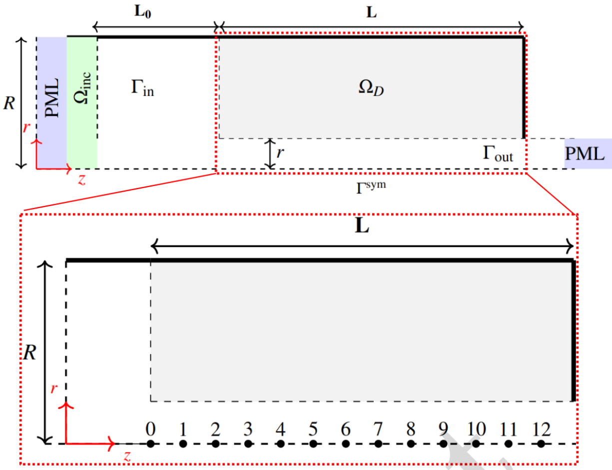

Figure 1: Simulation setup for optimization in COMSOL Multiphysics. Ω_{inc} represents the background pressure domain in the Pressure Acoustics module. The objective is to maximize the sum of pressure along 13 discrete points while imposing lower and upper bounds [15].

Pressure constraints are applied at all points except the SBH exit to prevent the design from converging toward a transmission-based SBH optimization.
The optimization is carried out over the frequency range from 400 Hz to 1000 Hz in steps of 50 Hz, accounting for the cutoff frequency of the axisymmetric waveguide. The dimensions of the design space are defined as: length of the design space ($L = 0.126\ m$), inlet channel width ($R = 0.115\ m$), outlet channel width ($r = 0.0015\ m$), and inlet length ($L_0 = 1\ m$).
The cost function of the optimization is given by

$$\begin{aligned} \max_{\zeta} \quad & J_p = \frac{1}{N} \sum_{n=1}^{13} \sum_{m=1}^{13} P_{i,j} \\ \text{s.t.} \quad & l_{n,m} \leq P_{n,m} \leq u_{n,m} \\ & 0 \leq \zeta(\mathbf{x}) \leq 1. \end{aligned} \tag{5}$$

where $l_{n,m}$ and $u_{n,m}$ denote the lower and upper bound constraints for the pressure P at each discrete spatial location n and frequency index m, respectively. The cost function is evaluated for a total of 13 spatial locations and 13 frequency points.

2.1. Results and Discussions

As shown in Figure 2a, the convergence of the cost function exhibits oscillations due to the large number of constraints. During the optimization process, the highest objective function values are associated with structures exhibiting partial transmission coefficients, indicating that optimizing the internal pressure leads to SBH-like devices with improved wave-focusing performance [15]. Optimized designs with broadband transmission coefficients are associated with moderate objective values, which are observed near iteration 390, as shown in Figure 2b. In this work, we focus on validating the optimized shape with broadband transmission for enhancing the detection of weak signals

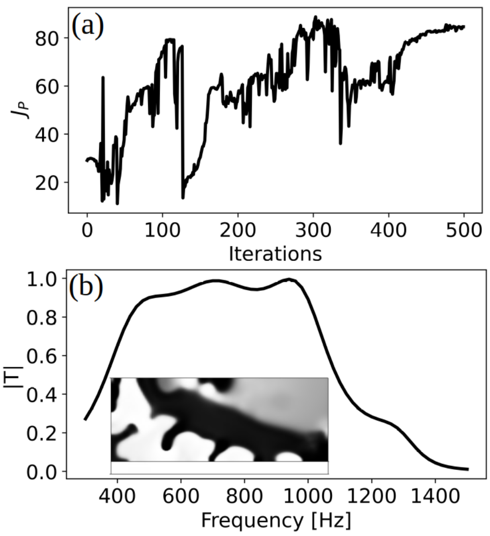

Figure 2: (a) Convergence of the objective value over 500 iterations. (b) Transmission coefficient of intermediate designs at iteration 390. The inset shows the intermediate shape with intermediate densities.

in a 2D axisymmetric domain, while the discussion of SBH structures with partial transmission is provided in Ref. [15].

The optimized shape, as shown in Figure 3a, contains intermediate densities, which are converted into solid regions using a threshold value of 0.5. Replacing the end condition of the optimized SBH with a sound-hard boundary allows for enhanced wave focusing. Therefore, transient analysis was carried out in a free field using COMSOL Multiphysics by placing the post-processed optimized structure 9.01 m from the source to evaluate the enhancement of weak signals.

A receiver was positioned inside the design to measure the pressure enhancement, and for comparison, the pressure was also measured at the same location without the SBH. The boundary was excited using a normal velocity to mimic a speaker emitting a Gaussian-modulated sinusoidal pulse with a center frequency of 750 Hz. Since the source size is smaller than the wavelength, a spherical wave is generated, and its amplitude decreases with distance due to geometric spreading. Perfectly matched layers were set on the external boundaries to minimize boundary reflections, as shown in Figure 3b (red color).

To validate the measurements, the floating features of the design were connected to the main structure using ribs. The rib thickness was kept to a minimum to avoid altering the acoustic response of the SBH at higher frequencies while maintaining structural rigidity. Due to the large dimensions of the structure (with outer diameter and length of 0.23 m and 0.126 m) respectively, which exceed the printer size and require a substantial amount of printing material, the sample was scaled down by 30% without compromising its performance, taking advantage of the scalability in acoustics.

Due to the complexity of the geometry, the samples were manufactured in separate parts using fused deposition modeling and subsequently assembled using adhesive to ensure that no gaps existed between the connected parts. Acrylonitrile butadiene styrene (ABS) filament was used for additive manufacturing due to the higher rigidity of the material compared with air. To measure the pressure inside the SBH, a hole with a diameter matching the outer diameter of a 1/2-inch B&K microphone was created, as shown in Figure 5a. Without loss of generality, an exact replication of the numerical setup in the experiment was not possible due to the size constraints of the isolation room.

Measurements were conducted over a broadband frequency range (up to 4000 Hz) by exciting the speaker with broadband white noise. The microphone was first placed 1.5 m in front of the speaker to measure the pressure without the SBH, and the measurement was then repeated with the microphone positioned inside the SBH, as shown in Figure 5b. Due to the geometric scaling, the frequency range of interest shifted to higher frequencies (1500–3000 Hz).

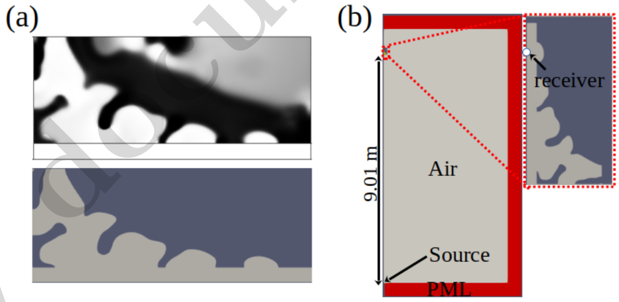

Figure 3: (a) Optimized design with intermediate densities and the corresponding post-processed final design adopted from Ref. [15]. (b) Numerical simulation setup for free-field measurements with a receiver placed inside the SBH.

For the numerical simulations, the received signal in the far field exhibits significant attenuation due to geometric spreading. Compared to the source signal shown in Figure 4a, the received signal is several orders of magnitude smaller, representing weak signals, as shown in Figure 4b. Detection of such signals with conventional sensors is often masked by background noise and the sensitivity limits of microphones. However, by placing the probe inside the SBH the recieved signal amplitude is enhanced up to 20 dB, as shown in Figure 4c.

As an exact replication of the numerical simulation was not feasible, the microphone position was kept fixed during the free-field measurements, and reflections from the walls were not explicitly accounted for. This approach assumes consistency across measurements to validate the weak signal enhancement capabilities. The received signals were transformed into the frequency domain using the Fast Fourier Transform, and the sound pressure level was calculated as $20\log_{10}(p/p_{\text{ref}})$, where p and p_{ref} denote the measured

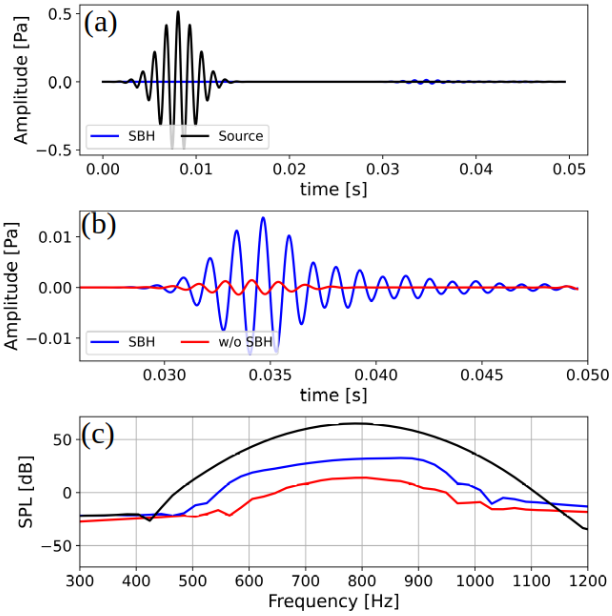

Figure 4: Numerical simulation in a free field: (a) source and received signals with and without the SBH; (b) close-up view of the received signals; and (c) corresponding sound pressure level comparison.

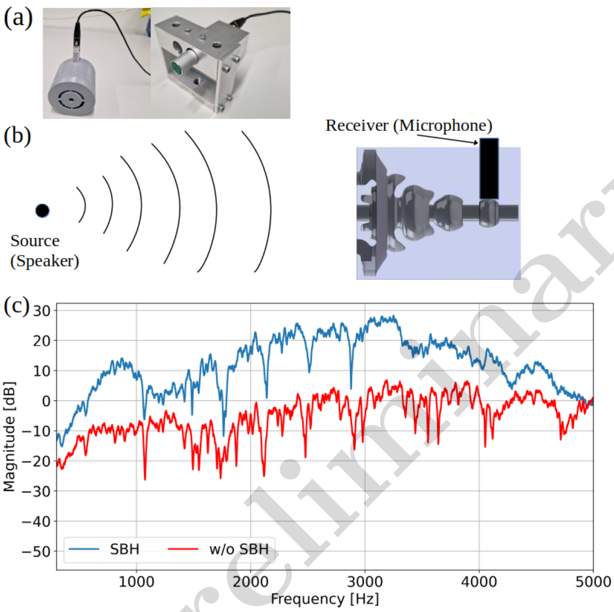

Figure 5: (a) Microphone placed inside the SBH with a holder for positional stability. (b) Schematic representation of the experimental setup. The microphone was placed 1.5 m away from the source for both cases (with and without SBH). (c) Corresponding sound pressure level comparison.

pressure and the reference pressure (2×10^{-5} Pa), respectively. Due to the scaling of the original geometry, the transmission coefficient is expected to shift toward higher frequencies, where weak signal enhancement is observed as shown in Figure 5c. Nonetheless, the results demonstrate that pressure enhancement inside the SBH significantly improves the detection of the source over a broad frequency range. This improvement is evident when compared with the case without the SBH, where the received signal remains weak. By placing the SBH closer to the source, the original signal can be recovered and even amplified by an order of magnitude. It should be noted that this work focuses primarily on maximizing the received signal before it reaches the microphone to enhance detection, while the properties of the microphone are not considered during the optimization process. In future work, microphone characteristics, such as impedance and a flat frequency response, can be incorporated into the optimization process in addition to maximizing the pressure amplification inside the SBH for practical applications. Furthermore, the size of the SBH can be further reduced to enable compact SBH devices for weak signal detection enhancement.

3. Conclusions

Based on the topology optimization of SBH wave-focusing devices, we numerically and experimentally validated the application of SBH-like devices for enhancing the detection limits of weak signals. The results demonstrate up to a 20 dB improvement in signal detection over a broad frequency range compared to measurements without the SBH. Beyond their conventional use as sound absorbers, exploiting the gradual increase in pressure within SBHs enables effective detection of weak signals. For an ideal SBH, where the pressure can theoretically become very large, the detection of extremely weak signals becomes feasible, which is essential in medical and nondestructive evaluation applications.

References

[1] J. Zhang, W. Rui, C. Ma, Y. Cheng, X. Liu, and J. Christensen, "Remote whispering metamaterial for non-radiative transceiving of ultra-weak sound," *Nature Communications*, vol. 12, no. 1, p. 3670, 2021. DOI: 10.1038/s41467-021-23991-3.

[2] Y. Chen, H. Liu, M. Reilly, H. Bae, and M. Yu, "Enhanced acoustic sensing through wave compression and pressure amplification in anisotropic metamaterials," *Nature communications*, vol. 5, no. 1, p. 5247, 2014.

[3] T. Chen, D. Yu, B. Wu, and B. Xia, "Weak signals detection by acoustic metamaterials-based sensor," *IEEE Sensors Journal*, vol. 21, no. 15, pp. 16 815–16 825, 2021.

[4] T. Chen, C. Wang, and D. Yu, "Pressure amplification and directional acoustic sensing based on a gradient metamaterial coupled with space-coiling structure," *Mechanical Systems and Signal Processing*, vol. 181, p. 109 499, 2022. DOI: 10.1016/j.ymssp.2022.109499.

[5] V. V. Krylov, “New type of vibration dampers utilising the effect of acoustic ”black holes”,” 2004. DOI: https://hdl.handle.net/2134/11851.

[6] V. V. Krylov, “Propagation of plate bending waves in the vicinity of one-and two-dimensional acoustic ‘black holes’,” Loughborough University, Tech. Rep., 2007. DOI: 10.13140/RG.2.1.4425.6484.

[7] M. A. Mironov, “Propagation of a flexural wave in a plate whose thickness decreases smoothly to zero in a finite interval,” *Soviet Physics Acoustics*, vol. 34, pp. 318–319, 1988.

[8] J. Zhao et al., “Broadband acoustic black hole for wave focusing and weak signal sensing,” *Applied Acoustics*, vol. 200, p. 109 078, 2022.

[9] W. Huang, H. Ji, J. Qiu, and L. Cheng, “Wave energy focalization in a plate with imperfect two-dimensional acoustic black hole indentation,” *Journal of Vibration and Acoustics*, vol. 138, no. 6, p. 061 004, 2016.

[10] Y. Chen, K. Yu, Q. Fu, J. Zhang, and X. Lu, “Modeling and analytical solution of an ideal continuum sonic black hole,” *Applied Mathematical Modelling*, vol. 141, p. 115 903, 2025.

[11] A. Mousavi, M. Berggren, and E. Wadbro, “How the waveguide acoustic black hole works: A study of possible damping mechanisms,” *The Journal of the Acoustical Society of America*, vol. 151, no. 6, pp. 4279–4290, 2022. DOI: 10.1121/10.0011788.

[12] A. Mousavi, M. Berggren, L. Hägg, and E. Wadbro, “Topology optimization of a waveguide acoustic black hole for enhanced wave focusing,” *The Journal of the Acoustical Society of America*, vol. 155, no. 1, pp. 742–756, 2024. DOI: 10.1121/10.0024470.

[13] S. B. Gebrekidan, F. Huber, F. Toth, S. Marburg, and M. Meader, “Experimental verification of acoustic wavefocusing of sonic black holes,” *Applied Physics Letters*, vol. 128, p. 122 202, 2026. DOI: 10.1063/5.0319258.

[14] H. H. Guilvaiee, A. Mousavi, M. Berggren, E. Wadbro, M. Kaltenbacher, and F. Toth, “Transient study of an optimized waveguide sonic black hole with wave focusing properties,” *Acta Acustica*, vol. 9, p. 36, 2025. DOI: 10.1051/aacus/2025019.

[15] S. B. Gebrekidan, F. Toth, S. Marburg, and M. Meader, “Versatile acoustic topology optimization of sonic black holes for enhanced wavefocusing,” *Applied acoustics*, vol. 249, p. 111 310, 2026. [Online]. Available: 10.1016/j.apacoust.2026.111310.

[16] M. B. Dühring, J. S. Jensen, and O. Sigmund, “Acoustic design by topology optimization,” *Journal of sound and vibration*, vol. 317, no. 3-5, pp. 557–575, 2008. DOI: 10.1016/j.jsv.2008.03.042.